Electron Transfer Behavior of Multi-Iron Sandwich-Type Polyoxometalates and Electrocatalytic Reduction Reactions

Bineta Keita,[a] Israel Martyr Mbomekalle,[a] Yu Wei Lu,[a] Louis Nadjo,*[a] Patrick Berthet,[b] Travis M. Anderson,[c] and Craig L. Hill*[c]

Keywords: Polyoxometalates / Sandwich complexes / Iron / Cyclic voltammetry

The physicochemical and electrocatalytic behaviors of eight multi-iron Wells–Dawson sandwich-type polyoxometalates were studied with specific emphasis on the Fe^{III} centers. Magnetization measurements were used to identify and quantify the antiferromagnetic interactions between the edge-sharing Fe^{III} units. Electrochemical studies show the stepwise reduction of the Fe^{III} centers, in complete agreement with magnetization conclusions. The location of the potential of each wave depends on the pH of the solution, as well as the concentration and composition of the electrolyte. In addition, ion-pairing studies show there is a positive shift of the Fe^{III} centers with an increase in ion pairing (i.e. $K^+ > Na^+ > Li^+$). The electrocatalytic reduction of dioxygen and hydrogen peroxide is efficient for all the complexes. However, there is a pronounced increase in efficiency as the number of Fe^{III} centers in the complex increases (i.e. 4 $Fe^{III} > 3$ $Fe^{III} > 2$ Fe^{III}). The mixed-metal complexes [αββα-Na_{14}-$(Mn^{II}OH_2)_2(Fe^{III})_2(As_2W_{15}O_{56})_2$ and αββα-$Na_{14}(Mn^{II}OH_2)_2$-$(Fe^{III})_2(P_2W_{15}O_{56})_2$] are also efficient catalysts for the reduction of NO and HNO_2.

Introduction

Fundamental and applied studies on polyoxometalates (POMs for convenience) continue to grow unabated.[1−6] This is due, in part, to their proven value in catalysis and other areas, as well as their highly modifiable nature. Redox potentials, acidity, size, shape, polarity, and other properties can all readily be altered synthetically. Symmetries in the structures of the POMs result in the equivalence of several metal centers that are detectable, for example, by NMR spectroscopy on fully oxidized species, and by EPR and/or NMR spectroscopy on their reduced analogues.[7−13] This equivalence of the metal centers raises the following question about the molecular electrochemistry of these compounds: in the absence of other possible mechanistic complications, related usually to pH or ion pairing of the countercations, can it be expected that symmetry-equivalent metal centers will be reduced simultaneously, or will the interactions between adjacent metal centers induce a stepwise reduction?[14]

Despite the structural equivalence of the twelve metal centers in the α-$PW_{12}O_{40}^{3-}$ Keggin anion (Figure 1A), a stepwise reduction of the tungsten centers is observed.[8] EPR experiments on this species show that the added electron is delocalized (type II in the scheme proposed by Robin

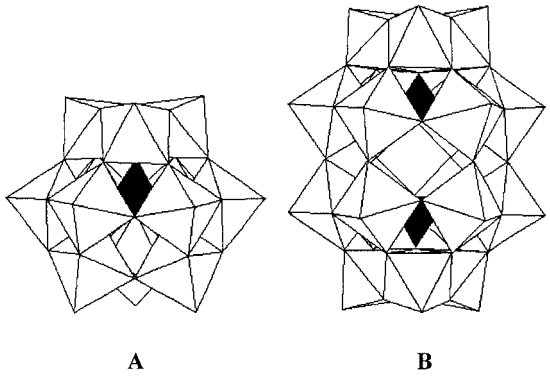

A B

Figure 1. Polyhedral representations of prototypical (A) Keggin (α-$XW_{12}O_{40}^{n-}$) and (B) Wells−Dawson (α-$X_2W_{18}O_{62}^{n-}$) anions

[a] Laboratoire de Chimie Physique, UMR 8000, CNRS, Université Paris-Sud,
Bâtiment 420, 91405 Orsay Cedex, France
Fax: (internat.) + 33-169154328
E-mail: nadjo@lcp.u-psud.fr
[b] Laboratoire de Physico-Chimie de l'Etat Solide, UMR 8648, CNRS, Université Paris-Sud,
Bâtiment 410, 91405 Orsay Cedex, France
[c] Department of Chemistry, Emory University,
Atlanta, Georgia, 30322, U.S.A.
Fax: (404) 727-6611
E-mail: chill@emory.edu
Supporting information for this article is available on the WWW under http://www.eurjic.org or from the author.

  DOI: 10.1002/ejic.200400099

and Day)[1,15] over all twelve tungsten centers suggesting that there is communication between the metal centers. In general, complete delocalization of the added electrons over all twelve metal centers appears to be the rule for all unsubstituted, highly symmetrical α-Keggin anions. Introduction of lower symmetry results in a variation in the degree of valence trapping.[10,11,13] Unlike the spherical α-Keggin anion, the Wells−Dawson structure (Figure 1B) is shaped like a prolate ellipsoid,[16] consisting of six "cap" tungsten centers and twelve "belt" tungsten centers. The non-equivalence of the "cap" and "belt" tungsten sites raises the issue of the initial site of the electron transfer. All the evidence supports the fact that the added electrons are first introduced into the "belt" tungsten sites.[9−13,17−23] Extended Hückel calculations provide a qualitative understanding of the initial electron transfer site in these compounds. In complete analogy with the Keggin model, a stepwise reduction of the equivalent metal centers is also seen in the Wells−Dawson POMs, with various degrees of valence trapping observed upon the introduction of other substituents such as d-electron-containing metal species.

Recently we reported the synthesis and electrochemical properties of the sandwich-type POM, αββα-$Na_{12}(Fe^{III}OH_2)_2(Fe^{III})_2(As_2W_{15}O_{56})_2$ (**Fe4As4**).[24] The accumulation of adjacent edge-sharing Fe^{III} centers in **Fe4As4** gives more favorable electrocatalytic properties to the complex than those observed in the monosubstituted complex, α_2-$As_2(FeOH_2)W_{17}O_{61}^{7-}$. Analogous complexes containing phosphorus heteroatoms (instead of arsenic) are known,[25−30] but the presence of arsenic facilitates the reduction of both Fe^{III} and W^{VI} centers. Preliminary studies of **Fe4As4** and its phosphorus analogue, αββα-$Na_{12}(Fe^{III}OH_2)_2(Fe^{III})_2(P_2W_{15}O_{56})_2$ (**Fe4P4**), indicate that both complexes show the stepwise reduction of the four antiferromagnetically coupled Fe^{III} centers in the central unit.[25] However, a comprehensive investigation of the equivalence of the heterometallic centers in the sandwich-type derivatives, highlighting their eventual interactions and rationalizing their electrochemistry, is lacking. We now report such a study. In the present work, magnetic measurements on several recently reported multi-iron Wells−Dawson sandwich-type POMs [including **Fe4As4**, **Fe4P4**, αααα-$Na_{16}(NaOH_2)_2(Fe^{III})_2(X_2W_{15}O_{56})_2$ [X = As^V (**Fe2As4**) or P^V (**Fe2P4**)], ααβα-$Na_{14}(NaOH_2)$-$(Fe^{III}OH_2)(Fe^{III})_2(X_2W_{15}O_{56})_2$ [X = As^V (**Fe3As4**) or P^V (**Fe3P4**)] and the mixed-metal complexes, αββα-Na_{14}-$(Mn^{II}OH_2)_2(Fe^{III})_2(X_2W_{15}O_{56})_2$ [X = As^V (**Fe2Mn2As4**) or As^V (**Fe2Mn2P4**)], see Figure 2 for structures] are used to identify and quantify the interactions between adjacent Fe^{III} (or Mn^{II}) centers, and electrochemical measurements illustrate how ion pairing, pH, and electrolyte compositions influence the redox properties of the complexes. In addition, these results show how the redox properties of the sandwich-type POMs are affected by the metal population of the central unit.[31] Specifically, the tetraferric complexes **Fe4As4** and **Fe4P4** are better than the diferric complexes **Fe2As4** and **Fe2P4** for the electrocatalytic reduction of dioxygen and hydrogen peroxide.

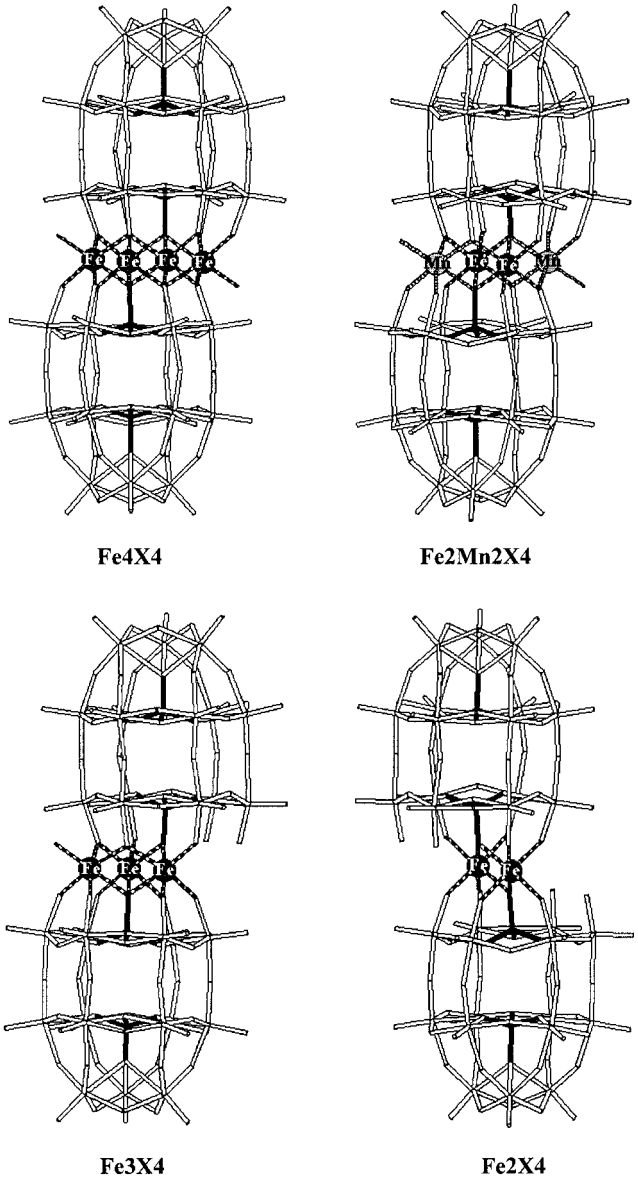

Figure 2. Combination wireframe/ball-and-stick representations of the eight multi-iron Wells−Dawson sandwich-type complexes studied here

Results and Discussion

Magnetic Studies

The crystallographic results of the present multi-iron sandwich-type complexes suggest that the arrangement of the Fe^{III} centers in edge-sharing octahedra will lead to electronic coupling between these metals.[24−27,29] Recently, we reported a detailed study of the magnetic properties of the arsenic complex, αββα-$Na_{12}(Fe^{III}OH_2)_2(Fe^{III})_2$-$(As_2W_{15}O_{56})_2$ (**Fe4As4**).[24] Here we report on the magnetic properties of the remaining complexes, which were all studied in a 0.1 T field. At 2 K, the magnetic moments per formula unit (for complexes **Fe4P4**, **Fe2As4**, **Fe2P4**, **Fe3As4**, **Fe3P4**, **Fe2Mn2As4**, and **Fe2Mn2P4**) are from three to seventy times lower than those expected for samples containing

the same number of non-interacting Fe^{III} or Mn^{II} ions. This is the first indication that antiferromagnetic interactions are present between the magnetic ions that form the central cluster. The magnetic moments decrease regularly with temperature for the trinuclear clusters (**Fe3As4** and **Fe3P4**), while shoulders or bumps are observed for the dinuclear (**Fe2As4** and **Fe2P4**) and tetranuclear (**Fe4P4**, **Fe2Mn2As4**, and **Fe2Mn2P4**) clusters. Plots of χT versus T were calculated from the experimental data in order to carry out a quantitative analysis of the magnetic interactions (Figure 3). For that purpose, the experimental susceptibility was written as shown in Equation (1), where χ_0 represents the temperature independent contributions due mainly to the diamagnetism of the ligands, and $\chi_{cluster}$ represents the intrinsic susceptibility of the cluster. The latter is given by Equation (2), in which the mean value $<S_T(S_T + 1)>$ depends on the temperature, which in turn determines the population of the energy levels resulting from individual spin coupling. These energy levels are eigenvalues of the magnetic Hamiltonian of the cluster. For the POMs under study here, the more general Hamiltonian is that describing the tetranuclear clusters (**Fe4As4**, **Fe4P4**, **Fe2Mn2As4**, and **Fe2Mn2P4**), while the related trinuclear (**Fe3As4** and **Fe3P4**) and dinuclear (**Fe2As4** and **Fe2P4**) clusters may easily be deduced from the former by setting the spin value of one or two of the metal ions to zero. Since the magnetic ions of the central tetranuclear clusters are found at the corners of an almost regular rhomboid, the magnetic interactions may be represented by two exchange constants, J_1 and J_2, which describe the interactions along the sides of the rhomboid and along its shortest diagonal, respectively (Scheme 1).

$$\chi_{mol} = \chi_{cluster} + \chi_0 \quad (1)$$

$$\chi_{cluster} = g^2 N\beta^2 <S_T(S_T + 1)> /3k\ T \quad (2)$$

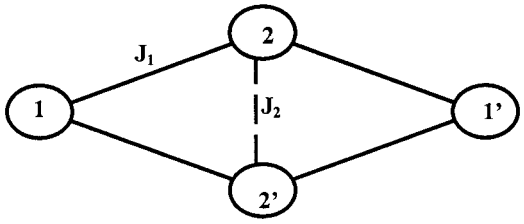

Scheme 1. Exchange pathways for the Fe_4 clusters

These interactions are of the superexchange type, and they are mediated by the two bridging oxygen atoms forming an edge shared by two neighboring FeO_6 or MnO_6 octahedra. Therefore, the magnetic energy of the cluster can be described by the following Heisenberg-type Hamiltonian [Equation (3)]. The eigenvalues of this Hamiltonian operator are obtained by the vector-coupling method of Kambe [Equation (4)],[32a] where S_{13}, S_{24}, and S_T are related with the spin operators $S_{13} = S_1 + S_3$, $S_{24} = S_2 + S_4$, and $S_T = S_{13} + S_{24}$. For a system of four ions with spin $S_i = 5/2$, there are 146 (S_T, S_{13}, S_{24}) combinations of energy E_i, whereas there are 27 and 6 combinations for systems with

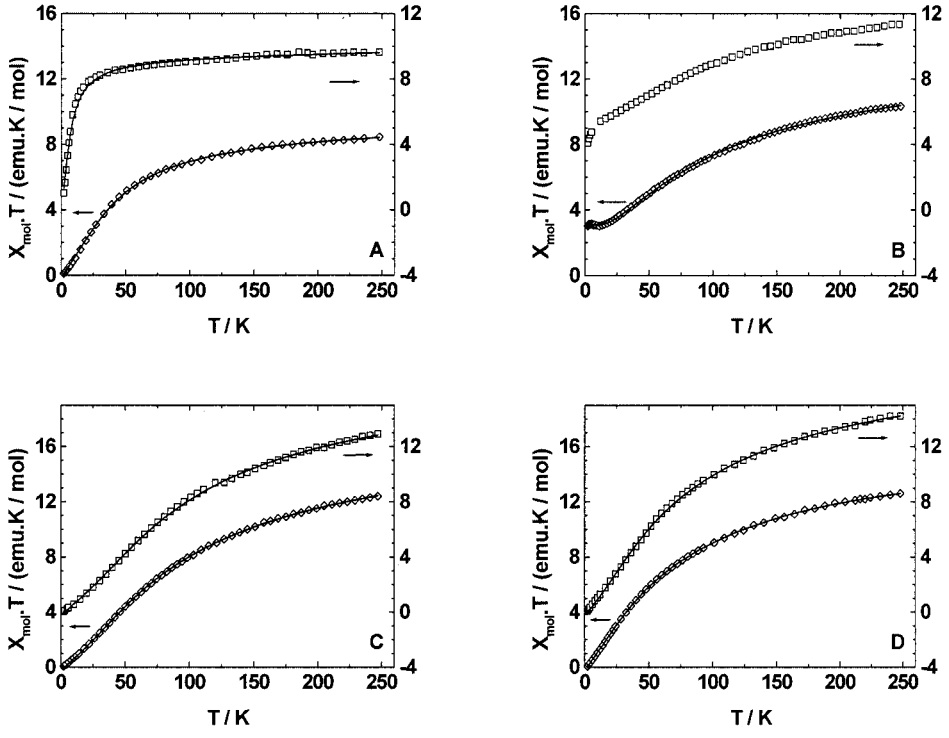

Figure 3. $\chi_{mol}T$ versus T plots for (A) **Fe2As4** and **Fe2P4**, (B) **Fe3As4** and **Fe3P4**, (C) **Fe4As4** and **Fe4P4**, and (D) **Fe2Mn2As4** and **Fe2Mn2P4**; the data corresponding to the phosphorus-based compounds are represented by squares, and the arsenic analogues are represented by diamonds; the continuous line represents the least-squares fit to the data using the parameters given in Table 1

three or two ions, respectively. After the calculation of these energies, the mean value of $<S_T(S_T + 1)>$ is obtained using Equation (5), with $b_i = 2S_T(E_i) + 1$ and $a_i = b_iS_T(Ei)$-$[S_T(E_i) + 1]$.

$$H = -2J_1(S_1S_2 + S_2S_3 + S_3S_4 + S_4S_1) - 2J_2S_1S_3 \quad (3)$$

$$E(S_T, S_{13}, S_{24}) = -J_1[S_T(S_T + 1) - S_{13}(S_{13} + 1) - S_{24}(S_{24} + 1)] - J_2[S_{13}(S_{13} + 1) - S_1(S_1 + 1) - S_3(S_3 + 1)] \quad (4)$$

$$<S_T(S_T + 1)> = \Sigma a_i \exp(-E_i/kT)/\Sigma b_i \exp(-E_i/kT) \quad (5)$$

The $\chi_M T$ versus T plots for all of the compounds are shown in Figure 3. It is possible to determine the magnetic parameters (g, J_1, J_2, $\chi_M T_{free}$, χ_0, E_0, and E_1) for each compound by fitting the calculated $\chi_{mol}T$ values to the experimental ones (Table 1). For **Fe4As4**, **Fe4P4**, **Fe2As4**, **Fe2P4**, **Fe2Mn2As4**, and **Fe2Mn2P4**, a small constant contribution $\chi_M T_{free}$ was subtracted from the experimental data before calculation. These contributions correspond to free Fe^{III} or Mn^{II} ions acting as countercations, or to fragments that occur as a result of some decomposition process taking place upon drying. Such a decomposition was reported by Coronado and co-workers for the closely related compound $\alpha\beta\beta\alpha$-$[(Mn^{II}OH_2)_2(Mn^{II})_2(P_2W_{15}O_{56})_2]^{16-}$.[32b] For most of the complexes under study here, the subtracted contributions represent less than 3% of the magnetic ions. However, for **Fe2P4**, this contribution represents nearly 17% of the magnetic ions, suggesting there is significantly more decomposition of this complex.

Examination of the values given in Table 1 confirms the antiferromagnetic nature of the interactions between the ions of spin $S_i = 5/2$. The ground states of complexes **Fe4As4**, **Fe4P4**, **Fe2As4**, **Fe2P4**, **Fe2Mn2As4**, and **Fe2Mn2P4** have a total spin of $S = 0$, whereas the ground state of **Fe3As4** is $S = 3/2$. For most complexes, the ground state is well separated (more than 5 cm^{-1}) from the first excited state. In complex **Fe3As4**, three antiferromagnetic interactions take place along the sides of a triangle; two of these interactions are described by J_1, and the third one by J_2. The orientations of the individual spins cannot simultaneously satisfy the constraints resulting from these interactions, and the system appears frustrated. Consequently, several configurations have close energies: the gap between $E_0(S_T = 3/2)$ and $E_1(S_T = 5/2)$ is 0.9 cm^{-1}, and that between E_0 and $E_2(S_T = 1/2)$ is 4.0 cm^{-1}. The values of the temperature-independent susceptibilities χ_0 are quite different from one complex to another and are sometimes positive. In addition, the Landé g-factors are close to 2 for all of the samples. A comparison of the interaction constants J_1 and J_2 shows that the interactions along an edge of the rhomboids are stronger than those interactions along the short diagonal. The structural data indicates first that the longest Fe−O distances are found along the diagonal bridges corresponding to J_2, and second, the lateral bridges corresponding to J_1 have longer Mn−O distances than Fe−O distances. Therefore, the differences between J_1(Mn−Fe), J_1(Fe−Fe), and J_2(Fe−Fe) may partially be explained by the M−O distances. However, the strength of these interactions also depends on the M−O−M bridging angles as well. The absolute value of J_2 determined for **Fe2P4** is lower than those obtained for the other complexes.[33] This low value accounts for the fast increase in $\chi_{mol}T$ at low temperature. This particular behavior was confirmed on a second sample from another batch, but it cannot be explained from the structural characteristics of the dinuclear unit, which are very close to those of **Fe2As4**. This suggests that some prominent modifications may have taken place when the product was dried, which is also consistent with the high value of χT_{free}. Attempts to fit the magnetic parameters of **Fe3P4** were unsuccessful. This is most likely due to the presence of a small amount of **Fe2P4** in the measured sample, which could explain the difference observed at low temperature between the $\chi_{mol}T$ product of **Fe3P4** and that of **Fe3As4**. However, this difference disap-

Table 1. Magnetic parameters and first energy levels of the compounds under study

Compound	**Fe2P4**	**Fe2As4**	**Fe3As4**	
g	2.07	2.03	2.04	
J_1/cm^{-1}	−	−	−4.76	
J_2/cm^{-1}	−0.50	−2.95	−2.47	
χT_{free} /emu K mol^{-1}	1.50	0.25	0.	
χ_0/emu mol^{-1}	1.48 10^{-3}	1.31 10^{-3}	−1.30 10^{-4}	
E_0/cm^{-1} [S_T]	−8.7 [0]	−51.6 [0]	−112.8 [1.5]	
$E_1 - E_0/cm^{-1}$	1.0	5.9	0.9	
Compound	**Fe4P4**	**Fe4As4**	**Fe2Mn2P4**	**Fe2Mn2As4**
g	2.05	2.03	2.07	1.99
J_1/cm^{-1}	−4.76	−4.70	−3.63	−3.54
J_2/cm^{-1}	−2.04	−2.98	−2.51	−3.37
χT_{free} /emu K mol^{-1}	0.50	0.19	0.53	0.58
χ_0/emu mol^{-1}	−4.4 10^{-4}	−9.7 10^{-4}	−5.6 10^{-8}	−1.9 10^{-3}
E_0/cm^{-1} [S_T]	−260.1 [0]	−244.7 [0]	−185.9 [0]	−170.3 [0]
$E_1 - E_0/cm^{-1}$ [S_T]	9.5	9.3	7.2	7.1

pears at higher temperature, suggesting that the magnetic interactions in both complexes are rather similar.

The susceptibilities of the tetranuclear clusters (**Fe4As4**, **Fe4P4**, **Fe2Mn2As4**, and **Fe2Mn2P4**) are very close to one another. With the use of the fitted parameters, the susceptibilities of **Fe4As4** and **Fe4P4** were extrapolated to 300 K, which gives 13.6 and 13.1 emu K mol^{-1}, respectively, for the $\chi_{mol}T$ products. These values are close to the calculated value of 13.3 emu K mol^{-1}, determined from the effective moment of **Fe4P4**, 10.3 μ_B, measured at 300 K by Zhang et al.[25]

pK_a Studies

To assess the stability of each of these complexes over a relatively large pH domain, we first determined their apparent pK_a values. In addition to the potential proton mobility of the water molecules fixed on the external $Fe^{III}-OH_2$ sites, protonatable sites might exist on the α-$X_2W_{15}O_{56}^{12-}$ (where X = As^V or P^V) unit itself. Measurements were performed with a 0.025 M solution of LiOH. The presence of Li^+ also helps to ensure the complete solubility of the samples. Experimental curves for all of the complexes are provided in the Supporting Information.[34]

Table 2 summarizes the results for complexes **Fe4As4**, **Fe4P4**, **Fe2As4**, **Fe2P4**, **Fe3As4**, and **Fe3P4**. The pK_a values are consistent with values reported for other similar sandwich-type complexes. Titration of the POMs without previous addition of acid gives similar results, and the results suggest that the number of mobile protons corresponds to the number of water molecules on the external Fe^{III} centers. Specifically, there are two, one, and zero mobile protons for complexes **Fe4As4** (and **Fe4P4**), **Fe3As4** (and **Fe3P4**), and **Fe2As4** (and **Fe2P4**), respectively. The pK_a values for the ionizable protons are comparable for similar complexes.[35−37] The number of protonatable sites on the POM framework itself seems to depend critically on the structure and, presumably, on the electronic interactions within the sandwich-type complexes. However, this behavior was not examined in more acidic solutions (less than pH = 2.5). It is also worth noting that the pK_a values do not smoothly increase as the pH of the solution is increased (and the POM deprotonated); in addition, the increase in the negative charge on the POM as a result of deprotonation causes an inversion in the observed pK_a values between the multi-iron sandwich complexes. This behavior has previously been observed in other POMs.[38−40] Finally, we note that the same acid−base properties are observed for both P and As heteroatoms.[41]

Electrochemical Studies

All of the compounds studied here are stable, at least in the timescale of the voltammetric studies, in the pH = 5 buffer medium (1 M CH_3COOLi and CH_3COOH) selected for these studies. The electrochemistry of the lacunary species (α-$P_2W_{15}O_{56}^{12-}$ and α-$As_2W_{15}O_{56}^{12-}$) were previously described.[24,42−44] There are positive potential shifts of the waves of α-$As_2W_{15}O_{56}^{12-}$ relative to those of α-$P_2W_{15}O_{56}^{12-}$ (20 mV and 54 mV for the first and second waves, respectively).[45] In contrast with the voltammograms of α-$As_2W_{15}O_{56}^{12-}$ and α-$P_2W_{15}O_{56}^{12-}$, those of **Fe4As4** and **Fe4P4** show four new waves in the potential domain +0.2 to −0.5 V. Figure 4A shows the CVs of α-$P_2W_{15}O_{56}^{12-}$ and **Fe4P4**. The four new waves are attributed to the reduction of the four Fe^{III} centers within the sandwich complex. At pH 3 (2 M NaCl + HCl), the formal potentials for the Fe^{III}/Fe^{II} redox couples are: 0.227, 0.124, −0.016 and − 0.093 V (vs. SCE), respectively. These potentials are distinctly more positive than the first W wave of α-$P_2W_{15}O_{56}^{12-}$ and **Fe4P4** (Figure 4A). This is consistent with the fact that Fe^{III} is known to reduce more easily than W^{VI} centers within substituted heteropolytungstates.[46] Corresponding data for the other complexes are included in the Supporting Information. The reduction of the W^{VI} centers is also influenced by the presence of the Fe^{III} centers in the sandwich molecule. The first wave of α-$P_2W_{15}O_{56}^{12-}$, which is slightly composite, splits into two waves in **Fe4P4**. This behavior is related to differences in the acid−base properties of the two POMs. Analogous to the CVs of α-$As_2W_{15}O_{56}^{12-}$ and α-$P_2W_{15}O_{56}^{12-}$, those of **Fe4As4** and **Fe4P4** are also very similar to each other. The presence of the arsenic heteroatom facilitates the reduction of both the Fe^{III} and W^{VI} centers (Figure 4B). The number of W^{VI} waves observed for **Fe4As4** or **Fe4P4**, and hence, the electron number for each wave, depends on the pH of the electrolyte. Rather classical electrochemical behaviors were observed for the W^{VI} centers in these complexes. Therefore, the focus of these studies will remain exclusively on the Fe^{III} centers. Figure 4C shows the stepwise reduction of the Fe^{III} centers in **Fe4P4**, with the potential domain restricted to that of the Fe^{III} redox processes. The X-ray crystal structures of **Fe4As4** and **Fe4P4** suggest that there are two types of symmetry-equivalent Fe^{III} centers.[24,25] There are two "external" Fe^{III} sites, which share two oxygen atoms with one α-$X_2W_{15}O_{56}^{12-}$ unit and three oxygen atoms with the other α-$X_2W_{15}O_{56}^{12-}$ unit. The sixth vertex of the octahedra is occupied by a water molecule. The sixth vertex of the two "internal" Fe^{III} sites is occupied by an additional

Table 2. Apparent pK_a values in 1 M LiCl at 25 °C for the multi-iron sandwich-type complexes

Heteroatom	X = As		X = P	
POM	Without added acid	With added acid	Without added acid	With added acid
Fe4X4 (X = As or P)	5.22, 5.42	5.32, 5.40	5.28, 5.80	5.17, 5.64
Fe3X4 (X = As or P)	5.62	2.54, 5.37	5.83	3.99, 5.86
Fe2X4 (X = As or P)	no titratable proton	2.76, 4.51, 3.58, 4.50	no titratable proton	2.19, 4.49, 3.82, 4.29

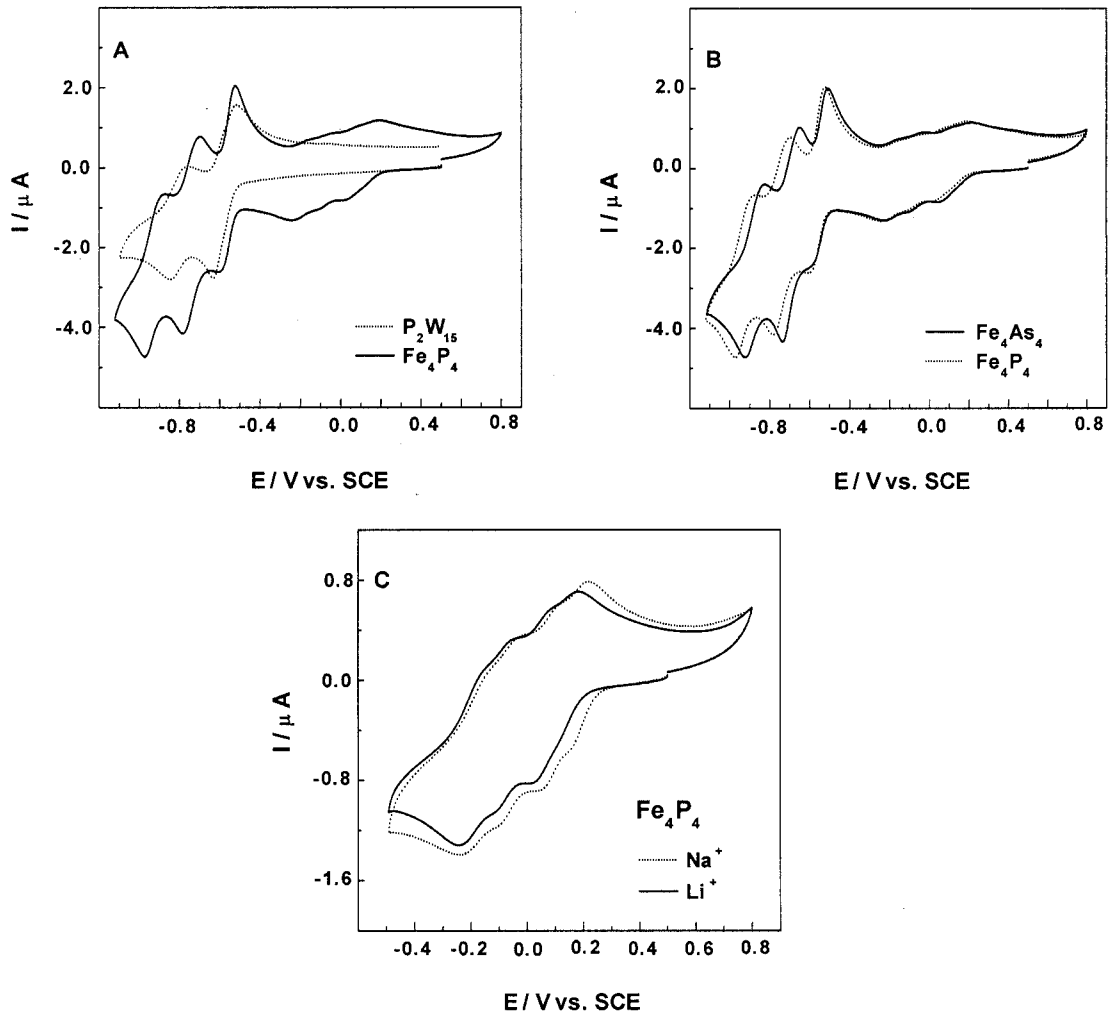

Figure 4. Cyclic voltammograms of **Fe4As4** and **Fe4P4** (2×10^{-4} M); the scan rate was 10 mV s^{-1}, the working electrode was glassy carbon, and the reference electrode was SCE; all measurements were performed in a 1 M CH_3COOLi + 1 M CH_3COOH (pH = 5) buffer solution except in (C), where the dotted line represents a measurement taken in a 0.5 M Na_2SO_4 + NaOH (pH = 5) buffer solution

oxygen atom from one of the two α-$X_2W_{15}O_{56}^{12-}$ units (rather than a water ligand). The structural data alone would suggest that there would be two groups of redox processes rather than four. The complete splitting into four distinct one-electron reduction processes suggests that there is some type of electronic communication involving the Fe^{III} centers.[47] This interaction must generate and/or reinforce inequivalence among the sites, especially in the reduced state; this is also consistent with the magnetic measurements. Finally, it is worth noting that all of the voltammetric patterns of **Fe4As4** and **Fe4P4** are perfectly well-defined and well-behaved at pH = 5. This observation is in contrast with the report that **Fe4P4** shows ill-defined waves with very small current intensities in media of pH > 4.[35] These differences may be due to differences in the media used to collect these measurements: this point was examined by running the CV in the same electrolyte (0.5 M Na_2SO_4 and NaOH, pH = 5) as that used in reference 35. The results in Figure 4C show that the waves remain perfectly well-defined (dotted line curve), and no decreased current is observed relative to the voltammogram recorded in acetate medium (solid line curve).

Ion Pairing

Although ion-pairing, pH, and ionic strength effects all exist simultaneously and act in competition, the data presented in Figure 4C allows the opportunity to discuss the first of these phenomena. In this system, an overall positive shift is observed for the Fe^{III} centers when a Na_2SO_4-based medium is used instead of CH_3COOLi. Since the two systems have the same ionic strength and pH (even though the buffer capacity is greater for CH_3COOLi), this positive shift must be due, in part, to the nature of the cation. It was previously shown that Na^+ engages in more intimate ion pairing with POMs than Li^+ since the hydrodynamic radius of Li^+ is greater than that of Na^+.[48,49] The positive shift of the potential for the Fe^{III} centers increases with increased ion pairing (i.e. $K^+ > Na^+ > Li^+$). For example, with both the pH and ionic strength kept constant, the formal potential measured for the Fe^{III}/Fe^{II} couple in

$Ge(FeOH_2)W_{11}O_{39}^{5-}$ is more positive with a Na^+ countercation than with Li^+. Complexes **Fe4As4** and **Fe4P4**, however, contain four Fe^{III} centers and could display more complex ion-pairing behavior. In addition, the two Fe^{III} sites with ionizable terminal water ligands further complicate the matter since ion-pairing and protonation can compete.[37] Figure 4C illustrates this complexity by showing that effects of the cation differ from one wave to the next. For example, the second and fourth redox couples (which are better behaved) experience a 35 mV shift and a negligibly small shift, respectively, with a change in medium from Na^+ to Li^+. The shift due to cation effects is larger for the first two redox couples. To further illustrate the competition between ion-pairing and protonation of the terminal water ligands, the pH of the system was lowered from five to three (prepared with 0.5 M Li_2SO_4 and H_2SO_4 or 0.5 M Na_2SO_4 and H_2SO_4). The results suggest that protonation supersedes ion-pairing with decreasing pH. These general trends are in good agreement with the apparent pK_a values measured previously. Complex **Fe4As4** gave results similar to **Fe4P4** under the same experimental conditions. The nature of the cation of the supporting electrolyte has a similar effect on the W^{VI} waves as described previously for monosubstituted Keggin derivatives.[37] For the remaining electrochemical studies, Na^+ is the countercation used since most of the POMs studied here were originally synthesized as the Na^+ salts.

pH Effects

The behavior of the W^{VI} waves of the POMs as a function of pH was the subject of several previous investigations.[1,4,37,43,46,50–52] Similar variations were observed within the present multi-iron sandwich-type derivatives, but they were not the focus of this particular study. We wished to determine how changes in pH affect the formal potentials of the Fe^{III} waves. Provisionally, it is worth noting that changes in pH might cause two or more of these waves to merge, although that phenomenon was not observed in these studies. For the present purpose, pH effects (from pH = 2 to pH = 7) were studied by adding an appropriate amount of concentrated mineral acid or base to a 2 M solution of NaCl. The high concentration of NaCl was used to minimize any effect induced by small ionic strength variations.

Figure 5 represents the variation in the formal potential between pH 2 and pH 7 for each of the Fe^{III} centers in **Fe4As4** and **Fe4P4**. The four Fe^{III} centers are numbered according to their formal potentials from the least negative (Fe1) to the most negative (Fe4). The formal potentials of the Fe^{III}/Fe^{II} redox couples do not vary smoothly with pH. Such an intricate pH dependence was described previously in the case of a single Fe^{III} center within monosubstituted Keggin derivatives.[37] Electronic communication between Fe^{III} centers in the sandwich-type derivatives might render the changes in their formal potentials pH interdependent, and possibly, might also render them more complex. Nevertheless, some new trends do appear in Figure 5. Focusing first on **Fe4As4**, the Fe1 and Fe2 centers show almost parallel formal potential changes; however, between pH 2–3 and pH 4–5 quasi-independent behavior is seen. The variation is almost linear above pH 5, with a slope of 55 mV/pH. In contrast, the formal potential for Fe3 is nearly independent for pH values up to 6, after which the potential begins to vary slightly. For Fe4, a linear dependence is observed from pH 3 to 5, with a slope of 26 mV/pH. At higher pH values, the potential is almost independent of pH. Although the present observations specifically concern the Fe^{III}/Fe^{II} redox couples and not only the Fe^{III} redox states, the variation in the formal potentials follow the trends expected based on the apparent pK_a values. In particular, the regions in which the formal potential is independent of pH are consistent with the possibility that ion pairing supersedes protonation. Furthermore, the formal potentials of the two internal Fe^{III} centers are not expected to depend directly on pH. The observed dependence must therefore be because of

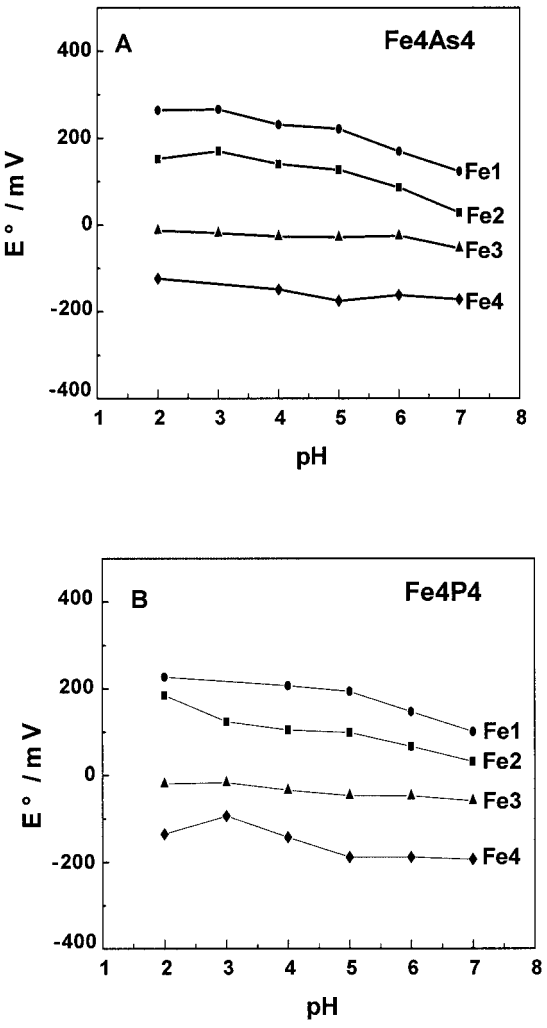

Figure 5. Plot of the formal potentials of **Fe4As4** (A) and **Fe4P4** (B) as function of pH for the four one-electron Fe^{III}-centered redox processes; the Fe^{III} centers are labeled FeX (with X = 1, 2, 3, or 4) from the most positive to the least positive reduction potential; the pH 2–3 solutions are comprised of 2 M NaCl + HCl, the pH 4–5 solutions are comprised of 2 M NaCl + 0.1 M CH_3COONa + 0.1 M CH_3COOH, and the pH 6–7 solutions are comprised of 2 M NaCl + 0.05 M NaH_2PO_4 + 0.05 M NaOH

the electronic communication between all of the Fe^{III} centers. The same trends were observed for **Fe4P4** as well, albeit small differences, which are presumably linked to differences induced by the different heteroatoms (As versus P) within these complexes. Finally, ion-pairing and pH effects converge during the reduction processes to suggest that the external Fe^{III} centers are reduced first. This is consistent with Pope's report on $(MnOH_2)_2(Mn)_2(PW_9O_{34})_2^{10-}$, in which it was discovered that oxidation first occurs at the Mn centers with water ligands.[53] However, due to the low intensity of the observed effects and to the fact that oxidation and reduction might involve different molecular orbitals, support (or invalidation) for the present hypothesis will be sought from complementary theoretical calculations.

Diferric and Triferric Sandwich-Type Complexes

Figure 6 shows the voltammograms of **Fe4As4**, **Fe3As4**, and **Fe2As4**, restricted to the waves attributed to the reduction of the Fe^{III} centers only. Several conclusions emerge from these patterns. For each CV, the number of waves corresponds to the number of Fe^{III} atoms in each complex. These observations suggest there are sufficiently strong interactions between the Fe^{III} centers in each of the complexes to induce complete splitting of their redox processes into separate steps. Qualitatively, the overall current intensities are also consistent with the number of Fe^{III} atoms in each complex. The number of Fe^{III} centers was also investigated by controlled potential coulometry measurements, which give three electrons per molecule for **Fe3As4** and **Fe3P4** and two electrons per molecule for **Fe2As4** and **Fe2P4** for the exhaustive reduction of these centers. At pH 3, the following values were determined: 3.95 ± 0.05 electrons per molecule for **Fe4As4** and **Fe4P4** at − 0.250 V (vs. SCE); 2.95 ± 0.06 electrons per molecule for **Fe3As4** and **Fe3P4** with the potential set at − 0.300 V (vs. SCE); 1.95 ± 0.07 electrons per molecule for **Fe2As4** and **Fe2P4** at − 0.360 V (vs. SCE). The CV patterns shift in the negative potential direction with a decrease in the number of Fe^{III} atoms. This is most likely related to the overall increase in the negative charge of the POM due to the decrease in the number of Fe^{III} atoms, and it is probably also related to the differences in pK_a in the reduced forms. The formal potentials measured from the CVs of the Fe^{III}/Fe^{II} centers within the complexes are included in the Supporting Information.

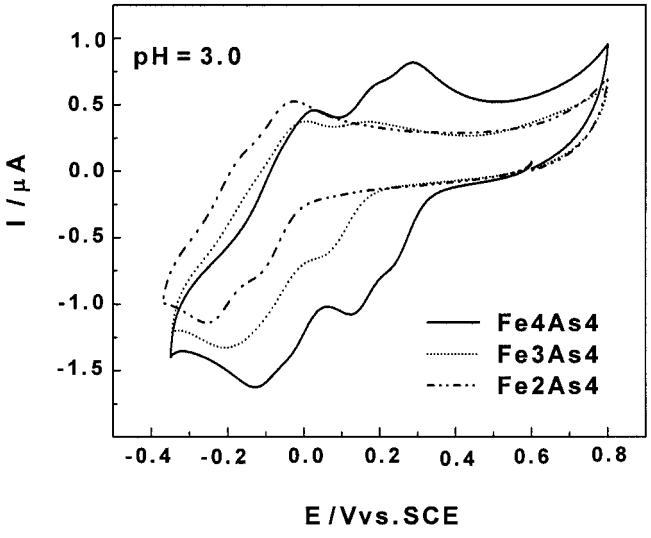

Figure 6. Cyclic voltammograms of **Fe4As4**, **Fe3As4**, and **Fe2As4** in 2×10^{-4} M, pH = 3 (2 M NaCl + HCl) buffer solution; the scan rate was 10 mV s^{-1}, the working electrode was glassy carbon, and the reference electrode was SCE

The relative potential shifts of the waves also seem to support the distinction between the external $Fe^{III}O_5(OH_2)$ centers and the internal $Fe^{III}O_6$ centers within the present complexes. Previously, we concluded that the external $Fe^{III}O_5(OH_2)$ centers are likely to be reduced before the internal $Fe^{III}O_6$ centers. Indeed, the CVs of **Fe3As4** and **Fe3P4** show the disappearance of a wave that can be attributed to an external $Fe^{III}O_5(OH_2)$ center in **Fe4As4** and **Fe4P4**. The CVs of **Fe2As4** and **Fe2P4**, which have no external $Fe^{III}O_5(OH_2)$ centers, also agree with this hypothesis since only two waves assigned to internal $Fe^{III}O_6$ centers are observed. These conclusions are also supported by the apparent pK_a values.

Mixed-Metal Sandwich-Type Complexes

Preliminary characterization of the mixed-metal multi-iron sandwich complexes indicated that they are stable from pH 0 to 7. In **Fe2Mn2P4**, the presence of Mn^{II} modifies the characteristics of the Fe^{III} and W^{VI} waves, which are observed at slightly more positive potentials than in **Fe2P4**. Figure 7 compares the Fe^{III}-based redox processes of complexes **Fe2P4** and **Fe2Mn2P4**. Controlled potential coulometry confirms that exhaustive reduction of these centers consumes 2.00 ± 0.05 electrons per molecule. Examination of Figure 7A shows that the first wave of **Fe2P4** is larger than that of **Fe2Mn2P4**, and that the first wave tends to merge with the second wave. Thus an ECE- or EEC-type process seems to be favored in the former complex. This observation leads to the conclusion that the reduced form of **Fe2Mn2P4** is less basic than the corresponding form of **Fe2P4**. The important influence of basicity is illustrated in Figure 7B. At pH 5, the two Fe^{III}-based waves merge in both complexes with coalescence being somewhat incomplete for **Fe2Mn2P4**, which shows a slightly composite wave.[54] The differences in the behavior of the arsenic analogues (complexes **Fe2As4** and **Fe2Mn2As4**) are less clear than those of the corresponding phosphorus analogues. The results indicate a clear influence of the central heteroatom, P or As, that consists (at pH 3) of an overall positive shift of the Fe^{III} waves without a current increase when P is replaced by As (see Supporting Information). A tentative explanation for this lack of change in the current is that the relevant pK_a values in the reduced forms of the As derivatives are very close from one complex to another.

A detailed study of the Mn^{II} wave in complex **Fe2Mn2P4** reveals, as expected, that the oxidation process becomes more difficult (i.e. moves towards more positive potentials) when the pH of the supporting electrolyte decreases. This point is illustrated for pH = 1 in Figure 7C where this process is kinetically sluggish. However, pre-treatment of the

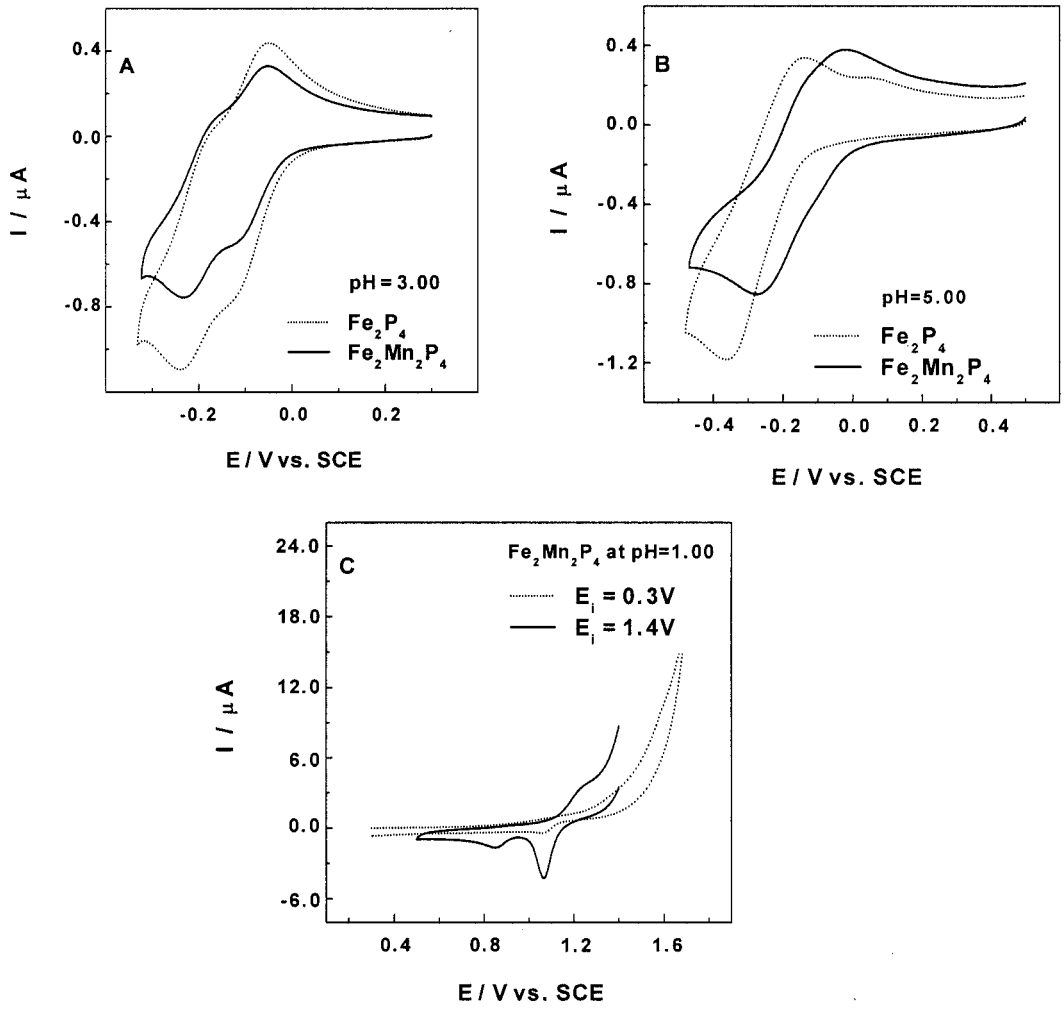

Figure 7. Cyclic voltammograms of **Fe2P4** and **Fe2Mn2P4** in different buffer solutions; the concentration of the POM was 2×10^{-4} M in all the solutions; the scan rate was 10 mV s^{-1}, the working electrode was glassy carbon, and the reference electrode was SCE; (A) comparison of **Fe2P4** and **Fe2Mn2P4** in a pH = 3 buffer (0.5 M Na_2SO_4 + H_2SO_4); (B) comparison of **Fe2P4** and **Fe2Mn2P4** in a pH = 5 medium (1 M CH_3COOLi +1 M CH_3COOH); (C) study of the Mn^{II} centers in **Fe2Mn2P4** in a pH = 1 medium (0.5 M Na_2SO_4 + H_2SO_4); E_i = initial potential; see the text for more details

electrode surface by pausing its potential at +1.4 V for a short time (120 s) prior to scanning the potential in the negative direction clearly reveals the presence of Mn^{II}. Under these conditions two reduction waves are observed, which are accompanied by a fairly well-behaved oxidation wave for the Mn^{II} centers on reversing the potential. This result is also shown in Figure 7C. Separation of the reduction into two steps is less pronounced in a pH 3 medium, where only a shoulder is observed. Examination of all these results together suggests that, for the two pH values we have explored (pH 3 and 5), the oxidation of Mn^{II} to Mn^{IV} is followed by the stepwise reduction of Mn^{IV} on reversing the potential. In addition, holding the potential at a selected positive value activates the electrode surface faster than continuous potential cycling. Continuous potential cycling of the electrode through the region in which the oxidation of interest is expected constitutes another technique in the activation of the glassy carbon surface electrode in the study of POM-based Mn^{II} centers. Steckhan and Sadakane found that this procedure gradually revealed the presence of the two waves of α-$Si(MnOH_2)W_{11}O_{39}^{6-}$ in a pH 6 phosphate buffer.[55] In contrast, we have previously shown that the merging of the two redox systems of Mn^{II} in α_2-$P_2(MnOH_2)Mo_2W_{15}O_{61}^{8-}$ results in a composite broad wave while cycling in a pH 6 phosphate medium (with concomitant deposition of an electroactive film on the electrode surface).[56]

Electrocatalysis

A pH 3 medium was selected for the studies on the electrocatalytic reductions of O_2 and H_2O_2. The efficiency of the catalytic process is evaluated by an excess parameter γ, which is defined as C° (O_2)/C° (POM) for dioxygen and C° (H_2O_2)/C° (POM) for hydrogen peroxide (C° = concen-

tration of the relevant species indicated in parentheses).[57] The catalytic efficiency (CAT) is defined as follows: CAT = [I (POM + O_2 or H_2O_2) − I^d (POM)]/I^d (POM), where I (POM + O_2 or H_2O_2) is the current for the reduction of the POM in the presence of O_2 or H_2O_2 and I^d is the corresponding diffusion current for the POM alone.

Figure 8A shows the CVs for **Fe4As4** in the absence and presence of dioxygen. The electrocatalytic reduction of O_2 starts after the second Fe^{III} reduction wave and precludes the possibility of observing other Fe^{III} reduction waves. This is consistent with the formation of an iron-dioxygen adduct upon reduction of the first two Fe^{III} centers. This adduct is subsequently reduced to give water with regeneration of the catalyst; an inner-sphere mechanism is likely to be operating. Water was confirmed to be the final product in the reduction of hydrogen peroxide by the same catalytic system. It is interesting that the final reduction process starts after the second Fe^{III} wave. Since the naked electrode does not reduce dioxygen in the potential region explored here, the reduced forms of the POM must drive the electrocatalytic process.[58] At the potential location of the second Fe^{III} wave, the number of electrons accumulated in the POM framework is not sufficient to carry out the overall process. Figure 8B compares the CVs of **Fe4As4**, **Fe3As4**, and **Fe2As4** in the presence of the same excess of dioxygen. The onset of the electrocatalytic process shifts in the negative potential direction when the number of Fe^{III} atoms decreases. Qualitatively, the catalytic efficiency follows the same trend. The reasons given before, which postulate an overall inner-sphere process remains valid here, even though an obvious binding site for dioxygen on **Fe2As4** is difficult to assign.

The electrocatalytic reduction of hydrogen peroxide by **Fe4As4** is shown in Figure 8C and compared with the reduction of dioxygen by the same system. The catalytic reduction of H_2O_2 is facile and occurs on the first Fe^{III} wave

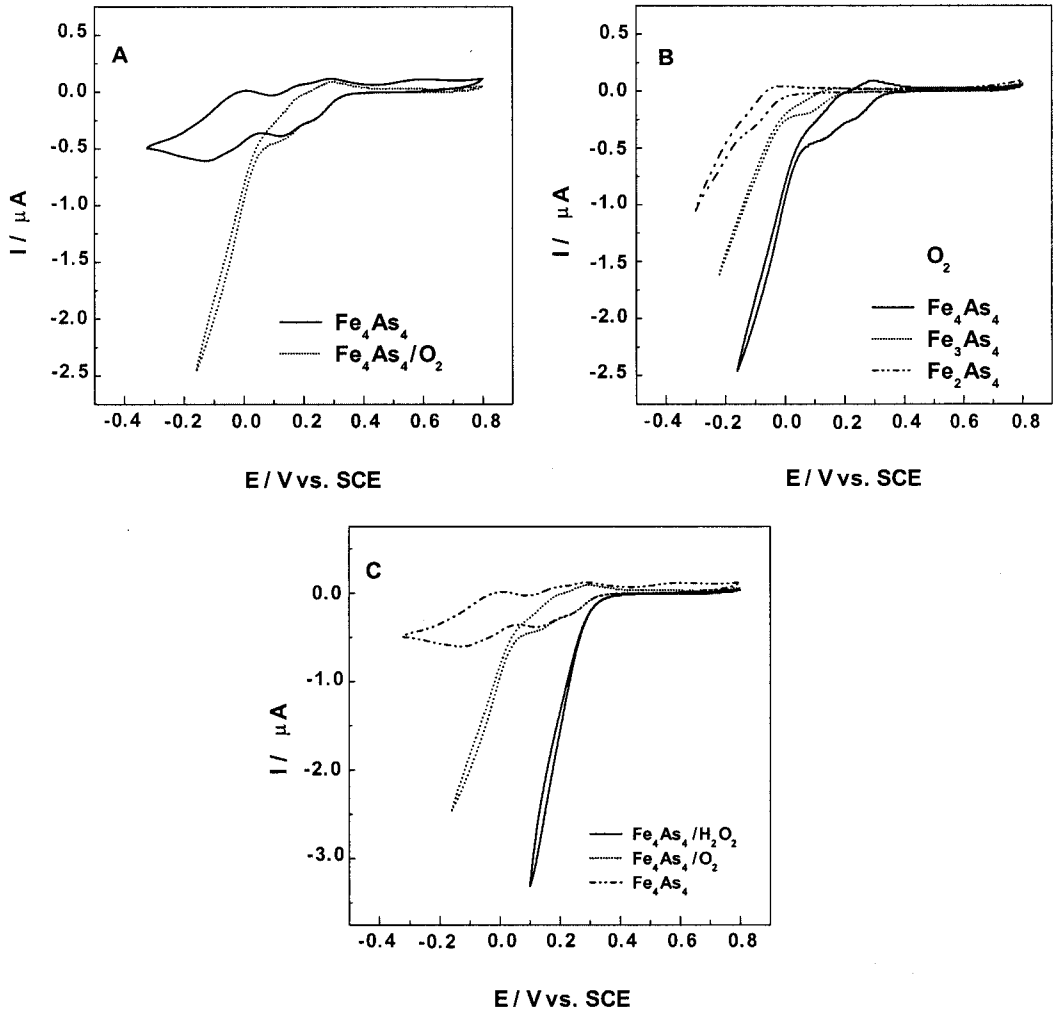

Figure 8. Cyclic voltammograms for the electrocatalytic reduction of dioxygen and hydrogen peroxide; the excess parameter for dioxygen or hydrogen peroxide was $\gamma = 5$, the scan rate was 2 mV s^{-1}, the working electrode was glassy carbon, the reference electrode was SCE, the concentration of the POM was 2×10^{-4} M, and the buffer had a pH of 3 (2 M NaCl + HCl); (A) electrocatalytic reduction with **Fe4As4**; (B) comparison of **Fe4As4**, **Fe3As4**, and **Fe2As4**; (C) comparison of the catalytic activity of **Fe4As4** towards dioxygen and hydrogen peroxide reduction

of **Fe4As4** at a potential much more positive than that observed for the electrocatalytic reduction of O_2. This observation indicates that the final reduction product of dioxygen is water. Complexes **Fe2As4** and **Fe3As4** give similar results, and the onset of the electrocatalytic process is seen to strictly follow the order of reduction of the three complexes.

Selected values of catalytic efficiencies (CAT) for the reduction of dioxygen and hydrogen peroxide are included in the Supporting Information. The general trends from Figure 8 are confirmed and quantified. Focusing specifically on complexes **Fe4As4** and **Fe4P4**, it appears that under the same experimental conditions, the phosphorus-containing complex **Fe4P4** is slightly more efficient than the arsenic analogue **Fe4As4** for the reduction of dioxygen, while the opposite is true for the reduction of hydrogen peroxide. This observation underscores the impossibility of anticipating which electrocatalyst would be more efficient when an inner-sphere pathway is operative. Three points deserve special emphasis. First, the electrocatalytic processes observed here remain efficient in other media. For example, at pH = 5, a CAT value of 523% was measured for the electrocatalytic reduction of O_2 by **Fe4P4** at a potential of −240 mV. This observation, and others not specifically described here, are important in that they establish the utility of the Fe^{III} centers within these multi-iron sandwich complexes in media of low proton availability. Second, we found that there is still ample room for optimization of the selected media for efficient electrocatalytic processes within these compounds. Third, despite the apparent superiority of **Fe4As4** and **Fe4P4** in the present voltammetric study, **Fe3As4** and **Fe3P4** might ultimately be the most useful long term catalysts, in part, due to their better stability under a wide range of conditions.[27,29]

Examination of these two electrocatalytic processes sheds some light on the reaction pathways. Dioxygen does not coordinate to Fe^{III} but it does coordinate to Fe^{II}. In the presence of only one Fe center [as in α_2-$As_2(FeOH_2)W_{17}O_{61}^{7-}$], no electron source is available immediately after the reduction potential of Fe^{III} to drive the catalytic process to completion. This observation underscores the importance of the accumulation of Fe^{III} centers, which carry out immediate further reduction of the adduct. It is also important to note that the accumulation of these catalytic centers decreases the overall negative charge of the POM, rendering its reduction more facile, and ultimately, saving energy during the electrocatalytic process. If H_2O_2 complexes with the Fe^{III} centers, then this might result in a favorable process for the electrocatalytic reaction. In support of this, complexes **Fe3As4** and **Fe3P4**, which have only one such exchangeable center, have approximately the same efficiency as α_2-$As_2(FeOH_2)W_{17}O_{61}^{7-}$ for the electrocatalytic reduction of H_2O_2.

Cooperativity Effects In Electrocatalytic NO_x Reduction

It is well established that Fe^{III}-substituted POMs catalyze the reduction of NO and/or NO_2^-.[58−60] The first step in this process is the formation of a complex with the Fe^{II} form of the POM and nitrogen oxide.[31,58] The actual catalytic reduction of this complex takes place with remarkable enhancement of the current intensity at more negative potentials where a large number of supplementary electrons accumulate in the W framework. With the goal of saving energy by moving the electron reservoir closer to the Fe^{III}-reduction potential, we have previously synthesized several Wells−Dawson-type monosubstituted derivatives, including α_1-$P_2(FeOH_2)W_{17}O_{61}^{7-}$ and α_2-$P_2(FeOH_2)Mo_2W_{15}O_{61}^{7-}$ in which the Fe- and W-waves or Fe- and Mo-waves merge in an appropriate pH media.[31,56] This strategy is favorable, and the entire catalytic process occurs at the reduction potential of the Fe^{III} center, which is now observed concomitantly with the Mo^{VI} or W^{VI} reduction waves. The same phenomenon is observed here. These results are illustrated briefly with **Fe2Mn2P4** in Figure 9, with $NaNO_2$ as the starting substrate. An important current intensity increase is observed with increasing γ values [γ is the excess parameter defined as γ = C° (NO_x)/C° (POM)] at the reduction potential of the Fe^{III} centers in a pH 1 solution.[61] In this potential region, no reduction is observed for NO or HNO_2 present in the solution.[62][63] Figure 9 shows unambiguously that the catalytic process begins simultaneously with the reduction of the Fe^{III} centers. Furthermore, it is worth noting the high efficiency of the electrocatalytic process, even though modest γ values were used. Finally, in the timescale of cyclic voltammetry, **Fe2P4** shows the same phenomenon as **Fe2Mn2P4** with regard to the electrocatalytic reduction of NO and NO_2^-. However, the latter complex might be a better choice for this catalytic process due to the greater stability of its Fe^{II} forms.[29] Under the same experimental conditions, **Fe2Mn2As4** also shows good catalytic efficiency for the reduction of nitrite. In addition, its activity at 0 V is 25% higher than that of **Fe2Mn2P4** as seen by the positive potential shift of the Fe^{III} waves in the former complex relative to the latter due to the different heteroatoms (i.e. As vs. P).

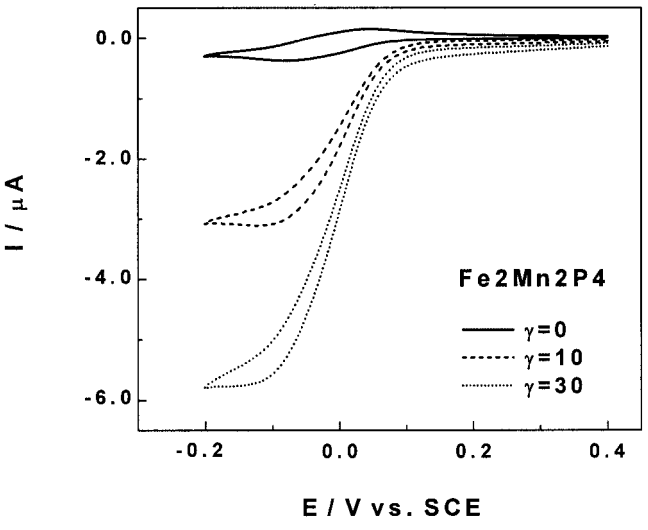

Figure 9. Cyclic voltammetric study of the electrocatalytic reduction of nitrite with a 2×10^{-4} M solution of **Fe2Mn2P4** in a pH = 1 medium (0.5 M Na_2SO_4 + H_2SO_4); the scan rate was 2 mV s^{-1}, the working electrode was glassy carbon, and the reference electrode was SCE

However, in a pH = 5 medium, the catalytic process (obtained with $NaNO_2$ as the starting substrate) is no longer observed in the iron reduction potential region, but rather it occurs in the reduction potential region of the first W wave. This observation is in full agreement with the expected absence of NO and HNO_2 in this medium. In contrast, experiments with pure NO[62,63] at pH = 5 show that the catalytic process starts directly in the potential region in which reduction of iron takes place . We have also examined the catalytic reduction of NO at pH = 1. All these results confirm that NO is the species that is electrocatalytically reduced by the present complexes throughout the evaluated pH region.

Conclusion

The X-ray crystallographic studies of **Fe4As4**, **Fe4P4**, **Fe2As4**, **Fe2P4**, **Fe3As4**, **Fe3P4**, and **Fe2Mn2P4** strongly suggest that electronic coupling exists between the Fe^{III} centers in this large class of multi-iron sandwich-type POMs. Magnetic studies corroborate this prediction and quantify these interactions in the oxidized states of the POMs. Electrochemical studies further indicate there is a stepwise reduction of the Fe^{III} centers. Ion-pairing studies show there is a positive shift of the Fe^{III} centers with increased ion pairing (i.e. $K^+ > Na^+ > Li^+$). Furthermore, ion-pairing and pH effects converge during the reduction processes to suggest that the external Fe^{III} centers of **Fe4As4** and **Fe4P4** are reduced before the internal Fe^{III} sites. Finally, electrocatalytic results show that the accumulation of Fe^{III} centers within a sandwich-type complex yield more favorable catalytic properties. This is attributable to the fact that there is a positive potential shift of the Fe^{III}-based redox processes associated with the accumulation of Fe^{III} centers, and in the case of the catalytic reductions of O_2, NO, or HNO_2, it also suggests that the presence of sites on the POM, which are likely to anchor the relevant molecule during its reduction, may also help to facilitate inner-sphere electron transfer.

Experimental Section

General Remarks: Samples of **Fe4As4**, **Fe4P4**, **Fe2As4**, **Fe2P4**, **Fe3As4**, **Fe3P4, Fe2Mn2As4**, and **Fe2Mn2P4** were obtained by published procedures,[25−27,29−30] and purity was confirmed by IR, elemental analysis, and cyclic voltammetry. Infrared spectra (1% by weight of POM in KBr) were recorded on a Perkin−Elmer Spectrum One FT-IR spectrometer. Measurements of pH and pK_a were performed with a Tacussel MVN 83 millivoltmeter-pH meter. Magnetic measurements were performed on a SQUID magnetometer, Quantum Design MPMS-5. The water content of the samples was measured by thermogravimetric analyses (TGA). All chemicals used were high purity grade and were used without further purification.

pK_a Studies: Measurements were carried out twice using LiOH (0.025 M) under the following conditions: after calibration of the experimental set-up, and standardization of the different reagent solutions, the initial 10 mL solution contained 5×10^{-4} M of the relevant POM dissolved in either pure 1.00 M LiCl or 1.00 M LiCl/3×10^{-3} M HCl. The measurement cell was thermostatted to 25 °C. The solutions were thoroughly deaerated with pure Ar, and the cell was kept under positive pressure at all times during the experiments.

Electrochemical Experiments: The pH values of the buffer solutions range from pH 2 to pH 7. Buffers between pH 2−3 are comprised of 2 M NaCl and HCl. Buffers between pH 4−5 are comprised of 2 M NaCl, 0.1 M CH_3COONa, and CH_3COOH, and buffers between pH 6−7 are made up of 2 M NaCl, 0.05 M NaH_2PO_4, and NaOH. Certain experiments required the use of more specialized buffer solutions. These buffer solutions are described in the text of the Results and Discussion. Solutions were deaerated with Ar for 30 min prior to measurements and kept under positive pressure at all times. Pure NO (N_2O grade) was purchased from Air Liquide (France). The concentration of POM in solution was 2×10^{-4} M, unless otherwise stated. The source, mounting, and polishing of the glassy carbon electrodes (GC, Tokai, Japan, 3 mm diameter) has been described in previous work.[31] The counter electrode was a platinum gauze of large surface area. The electrochemical apparatus was an EG and G 273A under computer control (M270 software). All experiments were performed at ambient temperature, and potentials are quoted against a saturated calomel electrode (SCE).

Acknowledgments

This work was supported in part by the University Paris XI and the CNRS (UMR, 8000 and 8648). We also thank the NSF (Grant CHE-0236686) for the research and Véronique Barra for running several experiments.

[1] M. T. Pope, *Heteropoly and Isopoly Oxometalates*, Springer-Verlag, Berlin, **1983**.
[2] M. T. Pope, A. Müller, *Angew. Chem. Int. Ed., Engl.* **1991**, *30*, 34−48.
[3] M. T. Pope, A. Müller, Eds., *Polyoxometalates: from Platonic Solids to Anti-Retroviral Activity*, Kluwer, Dordrecht, The Netherlands, **1994**.
[4] Topical issues on polyoxometalates: C. L. Hill (Editorial), *Chem. Rev.* **1998**, *98*, 1−389.
[5] M. T. Pope, A. Müller, Eds., *Polyoxometalate Chemistry: From Topology via Self-Assembly to Applications*, Kluwer, Dordrecht, The Netherlands, **2001**.
[6] T. Yamase, M. T. Pope, Eds., *Polyoxometalate Chemistry for Nano-Composite Design*, Nanostructure Science and Technology, Kluwer, Academic/Plenum Publishing, New York, **2002**.
[7] J. F. Keggin, *Proc. Roy. Soc.* **1934**, *A144*, 75−77.
[8] G. M. Varga Jr., E. Papaconstantinou, M. T. Pope, *Inorg. Chem.* **1970**, *9*, 662−667.
[9] C. Sanchez, J. Livage, J. P. Launay, M. Fournier, *J. Am. Chem. Soc.* **1983**, *105*, 6817−6823.
[10] M. Kozik, C. F. Hammer, L. C. W. Baker, *J. Am. Chem. Soc.* **1986**, *108*, 2748−2749.
[11] M. Kozik, C. F. Hammer, L. C. W. Baker, *J. Am. Chem. Soc.* **1986**, *108*, 7627−7630.
[12] M. Kozik, L. C. W. Baker, *J. Am. Chem. Soc.* **1990**, *112*, 7604−7611.
[13] N. Casañ-Pastor, L. C. W. Baker, *J. Am. Chem. Soc.* **1992**, *114*, 10384−10394.
[14] The problem of pure electron transfer reactions to and from molecules containing at least two identical redox centers has received appropriate attention in several studies. Two main classes are described: the first class of compounds are those cases in which non-interacting redox centers are present and for which successive electron transfers are expected to follow

simple statistics in the absence of coupled chemical steps. For example, see F. Ammar, J. M. Savéant, *J. Electroanal. Chem.* **1973**, *47*, 115−125; F. Ammar, J. M. Savéant, *J. Electroanal. Chem.* **1973**, *47*, 215−221; J. B. Flanagan, S. Margel, A. J. Bard, F. C. Anson, *J. Am. Chem. Soc.* **1978**, *100*, 4248−4253. The second group includes molecules in which various phenomena (including conjugation, ion pairing, solvation changes, and structural variations) induce or reveal interactions between the sites, and correlatively, differences between their half reaction potentials. These constitute the majority of published examples. For example, see A. J. Bard, *Pure Appl. Chem.* **1971**, *25*, 379−393; A. J. Bard, J. Phelps, *J. Electroanal. Chem.* **1970**, *25*, A2−A5; J. M. Fritsch, H. Weingarten, *J. Am. Chem. Soc.* **1968**, *90*, 793−795; C. P. Andrieux, J. M. Savéant, *J. Electroanal. Chem.* **1970**, *28*, 339−348; V. D. Parker, K. Nyberg, L. Eberson, *J. Electroanal. Chem.* **1969**, *22*, 150−152.

[15] The delocalized electron undergoes localization at low temperatures, otherwise the mixed valence compound is classified as type III under the scheme of Robin and Day.

[16] [16a] B. Dawson, *Acta Crystallogr.* **1953**, *6*, 113−126. [16b] H. D′Amour, *Acta Crystallogr., Sect. B* **1976**, *32*, 729−740.

[17] R. A. Prados, M. T. Pope, *Inorg. Chem.* **1976**, *15*, 2547−2553.

[18] J. L. Altenau, M. T. Pope, R. A. Prados, H. So, *Inorg. Chem.* **1975**, *14*, 417−421.

[19] R. Acerete, S. Harmalker, C. F. Hammer, M. T. Pope, L. C. W. Baker, *J. Chem. Soc., Chem. Commun.* **1979**, 777−779.

[20] L. Kazansky, M. Fedotov, *J. Chem. Soc., Chem. Commun.* **1980**, 644−646.

[21] A. Chemseddine, C. Sanchez, J. Livage, J. P. Launay, M. Fournier, *Inorg. Chem.* **1984**, *23*, 2609−2613.

[22] J. N. Barrows, M. T. Pope, *Inorg. Chim. Acta* **1993**, *213*, 91−98.

[23] B. Keita, Y. Jean, B. Lévy, L. Nadjo, R. Contant, *New J. Chem.* **2002**, *26*, 1314−1319.

[24] I. M. Mbomekalle, B. Keita, L. Nadjo, P. Berthet, K. I. Hardcastle, C. L. Hill, T. M. Anderson, *Inorg. Chem.* **2003**, *42*, 1163−1169.

[25] X. Zhang, Q. Chen, D. C. Duncan, C. Campana, C. L. Hill, *Inorg. Chem.* **1997**, *36*, 4208−4215.

[26] X. Zhang, T. M. Anderson, Q. Chen, C. L. Hill, *Inorg. Chem.* **2001**, *40*, 418−419.

[27] T. M. Anderson, X. Zhang, K. I. Hardcastle, C. L. Hill, *Inorg. Chem.* **2002**, *41*, 2477−2488.

[28] I. M. Mbomekalle, B. Keita, L. Nadjo, P. Berthet, W. A. Neiwert, C. L. Hill, M. D. Ritorto, T. M. Anderson, *Dalton Trans.* **2003**, 2646−2650.

[29] I. M. Mbomekalle, B. Keita, L. Nadjo, W. A. Neiwert, L. Zhang, K. I. Hardcastle, C. L. Hill, T. M. Anderson, *Eur. J. Inorg. Chem.* **2003**, 3924−3928.

[30] Dong and co-workers have also recently published the synthesis and characterization of **Fe4As4**, see: [30a] L. H. Bi, J. Y. Liu, Y. Shen, J. G. Jiang, E. K. Wang, S. J. Dong, *Gaodeng Xuexiao Huaxue Xuebao* **2002**, *23*, 472−474. [30b] L. Bi, J. Liu, Y. Shen, J. Jiang, S. Dong, *New. J. Chem.* **2003**, *27*, 756−764.

[31] B. Keita, F. Girard, L. Nadjo, R. Contant, R. Belghiche, M. Abbessi, *J. Electroanal. Chem.* **2001**, *508*, 70−80.

[32] [32a] K. Kambe, *J. Phys. Soc., Jpn.* **1950**, *5*, 48−51. [32b] C. J. Gómez-García, J. J. Borrás-Almenar, E. Coronado, L. Ouahab, *Inorg. Chem.* **1994**, *33*, 4016−4022.

[33] Recent calculations on the electronic transfer parameters in reduced phosphotungstates have given J values of 4000 cm^{-1}, while those observed in the eight complexes studied here are of the order of 2−5 cm^{-1}. For more information, see: N. Suaud, A. Gaita-Ariño, J. M. Clemente-Juan, J. Sánchez-Marín, E. Coronado, *J. Am. Chem. Soc.* **2002**, *124*, 15134−15140.

[34] For more information on general procedures for handling pK_a data, see [34a] A. E. Martell, R. J. Motekaitis, *Determination and Use of Stability Constants*, 2nd ed., VCH Publishers, Inc., New York, **1992**. [34b]M. T. Caudle, C. D. Caldwell, A. L. Crumbliss, *Inorg. Chim. Acta* **1995**, *240*, 519−525.

[35] L. Ruhlmann, L. Nadjo, J. Canny, R. Contant, R. Thouvenot, *Eur. J. Inorg. Chem.* **2002**, 975−986.

[36] R. Contant, M. Abbessi, J. Canny, A. Belhouari, B. Keita, L. Nadjo, *Inorg. Chem.* **1997**, *36*, 4961−4967.

[37] J. E. Toth, F. C. Anson, *J. Electroanal. Chem.* **1988**, *256*, 361−370.

[38] E. Papaconstantinou, M. T. Pope, *Inorg. Chem.* **1967**, *6*, 1152−1155.

[39] R. Contant, J.-M. Fruchart, *Rev. Chim. Miner.* **1974**, *11*, 123−140.

[40] B. Keita, Y. W. Lu, L. Nadjo, R. Contant, *Electrochem. Commun.* **2000**, *2*, 720−726.

[41] The present results differ substantially for at least one of the two pK_a values attributed by Ruhlmann and co-workers (ref.[35]) to the successive deprotonation of the two water molecules attached to the external metal atoms in αββα-$(MOH_2)_2(M)_2(P_2W_{15}O_{56})_2$ (M = Mn, Fe, Co, Cu, Zn, or Cd). In addition, the two pK_a values for **Fe2P4** are identical to those found for **Fe4P4**. However, the numbers for **Fe2P4** (even accounting for some experimental uncertainty) could only feature pK_a values for the protonable sites within the molecule.

[42] W. Song, X. Wang, Y. Liu, H. Xu, *J. Electroanal. Chem.* **1999**, *476*, 85−89.

[43] B. Keita, I. M. Mbomekalle, L. Nadjo, R. Contant, *Electrochem. Commun.* **2001**, *3*, 267−273.

[44] R. Contant, R. Thouvenot, *Can. J. Chem.* **1991**, *69*, 1498−1506.

[45] This observation is in agreement with the remark drawn from the study of α-$As_2W_{15}O_{56}^{12-}$ and α-$P_2W_{15}O_{56}^{12-}$ that the former species is easier to reduce than the latter, see B. Keita, I. M. Mbomekalle, L. Nadjo, R. Contant, *Eur. J. Inorg. Chem.* **2002**, 473−479.

[46] B. Keita, A. Belhouari, L. Nadjo, R. Contant, *J. Electroanal. Chem.* **1998**, *442*, 49−57.

[47] Although coupling between the Fe centers is invoked as an explanation for the separation (or lack thereof) of the various reduction waves, reduction of these centers (whether clearly sequential or not) may also depend simply on the effect of the extra negative charge taken on by the POM each time a Fe^{III} center is reduced to Fe^{II}. Literature has solved the case of the first reduction potentials of several Keggin species under conditions of no protonation. The correlation line has a slope of −0.18 V/unit charge (see ref.[1,18]). The same correlation was also suggested for select examples of second reduction potentials (see M. T. Pope, G. M. Varga Jr., *Inorg. Chem.* **1966**, *5*, 1249−1254). In the latter case, only highly symmetrical POMs with little or no ion pairing were addressed and the reduced centers were all W-based. In the multi-iron compounds we address here, electrons are localized essentially in the Fe_4 central unit where ion pairing is extensively operative and in competition with protonation. In addition, we have to consider the Wells-Dawson trivacant species as the precursors in the synthesis of the present sandwich complexes. Therefore only a semi-quantitative evaluation of this phenomenon can be made at best. However, the observation of a broad, single large cathodic current featuring the combined series of one-electron reduction processes of the four Fe centers made on $[Fe_4(OH_2)_{10}(β\text{-}XW_9O_{33})_2]^{n-}$ (n = 6, X = As^{III}, Sb^{III}; n = 4, X = Se^{IV}, Te^{IV}) in which Fe centers are not directly connected (ref.[51]) supports the idea of electronic communication between Fe centers. It can therefore be concluded that the stepwise addition of electrons required in molecular electrochemistry and the subsequent stepwise increase in the overall negative charge of the POM are not sufficient to split the waves measurably in a case where direct influence between structurally equivalent centers does not exist.

[48] Anson et al. (ref.[37]) have also shown that reduced forms of Fe^{III}-monosubstituted Keggin anions engage in ion-pairing with alkali metal cations.

[49] [49a] V. A. Grigoriev, C. L. Hill, I. A. Weinstock, *J. Am. Chem.*

Soc. **2000**, *122*, 3544−3545. [49b] V. A. Grigoriev, D. Cheng, C. L. Hill, I. A. Weinstock, *J. Am. Chem. Soc.* **2001**, *123*, 5292−5307.
[50] B. Keita, L. Nadjo, *Mater. Chem. Phys.* **1989**, *22*, 77−103.
[51] U. Kortz, M. G. Savelieff, B. S. Bassil, B. Keita, L. Nadjo, *Inorg. Chem.* **2002**, *41*, 783−789.
[52] L. Cheng, H. Sun; B. Liu, J. Lin, S. Dong, *Electrochem. Commun.* **1999**, *1*, 155−158.
[53] X. Zhang, G. B. Jameson, C. J. O′Connor, M. T. Pope, *Polyhedron* **1996**, *15*, 917−922.
[54] Such differences in the pK_a values of the two complexes might be explained by considering that **Fe2Mn2P4** should behave much like a saturated complex, while **Fe2P4** is more lacunary in nature.
[55] M. Sadakane, E. Steckhan, *J. Mol. Catal. A: Chem.* **1996**, *114*, 221−228.
[56] B. Keita, Y. W. Lu, L. Nadjo, R. Contant, M. Abbessi, J. Canny, M. Richet, *J. Electroanal. Chem.* **1999**, *477*, 146−157.
[57] B. Keita, M. Benaïssa, L. Nadjo, R. Contant, *Electrochem. Commun.* **2002**, *4*, 663−668.
[58] J. E. Toth, F. C. Anson, *J. Am. Chem. Soc.* **1989**, *111*, 2444−2451.
[59] B. Keita, L. Nadjo, R. Contant, M. Fournier, G. Hervé, (CNRS), *French Patent 89l1,728*, **1989**.
[60] B. Keita, L. Nadjo, R. Contant, M. Fournier, G. Hervé, (CNRS), *Eur. Patent Appl. EP 382,644*, **1990**; *Chem. Abst.* **1991**, *114*, 191882u.
[61] At pH = 1, the actual active species should be HNO_2 and/or NO. In fact, the following sequence is known: $HNO_2 \rightarrow H^+ + NO_2^-$ pK_a = 3.3 at 18 °C and HNO_2 disproportionates in fairly acidic solution: 3 $HNO_2 \rightarrow HNO_3$ +2 NO + H_2O. The rate of this reaction is known to be low.
[62] A. Belhouari, B. Keita, L. Nadjo, R. Contant, *New J. Chem.* **1998**, 83−86.
[63] B. Keita, A. Belhouari, L. Nadjo, R. Contant, *J. Electroanal Chem.* **1995**, *381*, 243−250.

Received February 6, 2004
Early View Article
Published Online June 17, 2004

